Condensed Matter Physics, 2001, Vol. 4, No. 1(25), pp. 149–160

Non-resonant Raman scattering through a metal-insulator transition: an exact analysis of the Falicov-Kimball model

J.K.Freericks [1,2] , T.P.Devereaux [3]

[1] Department of Physics, Georgetown University, Washington, DC 20057, USA

[2] Isaac Newton Institute, Cambridge CB3 0EH, UK

[3] Department of Physics, University of Waterloo, Waterloo, ON, Canada, N2l 3G1

Received August 14, 2000

For years, theories for Raman scattering have been confined to either the insulating or fully metallic state. While much can be learned by focusing attention on the metal or insulator, recent experimental work on the cuprate systems points to the desirability of formulating a theory for Raman response which takes one through a quantum critical point – the metal-insulator transition. Using the Falicov-Kimball model as a canonical model of a MIT, we employ dynamical mean-field theory to construct an exact theory for non-resonant Raman scattering. In particular we examine the formation of charge transfer peaks and pseudogaps as well as the low-energy dynamics. The results are qualitatively compared to the experimental B_{1g} Raman spectra in the cuprates, which probes the hot quasiparticles along the Brillouin zone axes. The results shed important information on normal state electronic transport and the pseudo-gap in the cuprates.

Key words: *Raman scattering, metal-insulator transition*

PACS: *78.30.-j, 71.30.+h, 74.72.-h*

1. Introduction

Raman scattering in the cuprate materials involves the inelastic scattering of light by electron-hole excitations of the correlated many-body system. It is a non-destructive bulk probe of the electron dynamics over a wide range of energy scales and temperatures. The experiments can discriminate between a number of different symmetries of the electronic system by polarizing the incoming light and measuring the reflected light with a polarized detector. Three principal symmetries are examined in the cuprate materials: A_{1g}, which has the full symmetry of the lattice (i.e. is s-like), and two d-like symmetries B_{1g} (which probes the Brillouin zone axes) and B_{2g} (which probes the Brillouin zone diagonals). While the Raman response for the A_{1g} and B_{2g} symmetries are closer to those of conventional metals, the B_{1g} response is anomalous, and has large spectral weight shifts as functions of doping and temperature [1]. It is believed by many workers in the field that this B_{1g} response is arising from the proximity of the cuprates to a quantum-critical point corresponding to a metal-insulator transition.

Theoretical treatments of non-resonant Raman scattering are rather complete for band metals [2] and insulators [3], but there is no theory that can successfully interpolate between these two limits to pass through the correlated metal-insulator transition. In this contribution, we show how an exact solution of the spinless Falicov-Kimball model [4] using dynamical mean field theory [5,6] provides a theoretical model that illustrates the generic behaviour of Raman response through the metal-insulator transition and interpolates between the known limits. We find that our Raman spectra show charge-transfer peaks and nontrivial low-frequency spectral-weight transfers that are indicative of the proximity to a quantum critical point and represent well the experimental data in the cuprates.

The Hamiltonian of the spinless Falicov-Kimball model [4] is

$$H = -\frac{t^*}{2\sqrt{d}}\sum_{\langle i,j\rangle} d_i^\dagger d_j + E_f\sum_i w_i - \mu\sum_i (d_i^\dagger d_i + w_i) + U\sum_i d_i^\dagger d_i w_i, \qquad (1)$$

where $d_i^\dagger$ (d_i) is the spinless conduction electron creation (annihilation) operator at lattice site i and $w_i = 0$ or 1 is a classical variable corresponding to the localized f-electron number at site i. The hopping matrix between the nearest neighbours $\langle i,j\rangle$ (on a hypercubic lattice in d-dimensions [5], with $d\to\infty$) is $-t^*/(2\sqrt{d})$ with t^* chosen as our energy unit, E_f is the localized electron level, μ is the chemical potential and U is the mutual electron repulsion when a conduction electron and a localized f-electron both occupy the same lattice site. We will adjust both E_f and μ so that the average filling of the d-electrons is 1/2 and the average filling of the f-electrons is 1/2.

The Raman response is found from a density-density correlation function

$$\chi_{\mathrm{Raman}}(\mathrm{i}\nu_l) = \sum_{\mathbf{k}}\int_0^\beta \mathrm{d}\tau \mathrm{e}^{\mathrm{i}\nu_l\tau}\left\{\frac{\mathrm{Tr}\, T_\tau\langle \mathrm{e}^{-\beta H}\rho_{\mathbf{k}}(\tau)\rho_{\mathbf{k}}(0)\rangle}{Z} - \left[\frac{\mathrm{Tr}\,\langle \mathrm{e}^{-\beta H}\rho_{\mathbf{k}}(0)\rangle}{Z}\right]^2\right\}, \qquad (2)$$

with the uniform ($\mathbf{q}=0$) Raman density operator

$$\rho_{\mathbf{k}} = \gamma(\mathbf{k}) d_{\mathbf{k}}^\dagger d_{\mathbf{k}}, \quad d_{\mathbf{k}} = \frac{1}{N}\sum_j \mathrm{e}^{-\mathbf{R}_j\cdot\mathbf{k}} d_j, \qquad (3)$$

$Z = \mathrm{Tr}\,\langle \mathrm{e}^{-\beta H}\rangle$, the partition function, and $\mathrm{i}\nu_l = 2\mathrm{i}\pi l T$ the Bosonic Matsubara frequency (the τ-dependence of the operators is with respect to the full Hamiltonian). The Raman scattering amplitude $\gamma(\mathbf{k})$ is a complicated function of the incoming and outgoing photon polarizations, of the photon energies, and the polarizability of the medium. In nonresonant Raman scattering (which we examine here) one neglects the frequency dependence of the Raman scattering amplitude, and characterizes the Raman response in terms of the different spatial symmetries of the remaining function $\gamma(\mathbf{k})$. One can expand this function in a Fourier series and examine the contributions of the lowest components of the series, and compare them to the experiment. More sophisticated approaches would calculate the Raman scattering amplitude from "first-principles" and would include any possible resonant Raman scattering effects. We leave those pursuits to future work.

2. Formalism

The Falicov-Kimball model can be solved exactly in the infinite-dimensional limit by using dynamical mean-field theory [6,7]. We summarize the main points to establish our notation. The local Green's function at the Fermionic Matsubara frequency $\mathrm{i}\omega_n = \mathrm{i}\pi T(2n+1)$ is defined by

$$G_n = G(\mathrm{i}\omega_n) = -\mathrm{Tr}\, T_\tau \int_0^\beta \mathrm{d}\tau \mathrm{e}^{\mathrm{i}\omega_n \tau} \frac{\langle \mathrm{e}^{-\beta H_{\mathrm{at}}} d(\tau) d^\dagger(0) S(\lambda)\rangle}{Z}, \tag{4}$$

with

$$Z = Z_0(\mu) + \mathrm{e}^{-\beta(E_f-\mu)} Z_0(\mu - U), \tag{5}$$

the atomic partition function expressed in terms of

$$Z_0(\mu) = \mathrm{Tr_d}\, \langle \mathrm{e}^{-\beta H_0} S(\lambda)\rangle, \quad H_0 = -\mu d^\dagger d. \tag{6}$$

In the above equations, the atomic Hamiltonian H_{at} is the Hamiltonian of equation (1) restricted to one site, with $t^* = 0$, and all time dependence is with respect to this atomic Hamiltonian. The evolution operator $S(\lambda)$ satisfies

$$S(\lambda) = \exp\left[-\int_0^\beta \mathrm{d}\tau \int_0^\beta \mathrm{d}\tau' d^\dagger(\tau)\lambda(\tau-\tau')d(\tau')\right], \tag{7}$$

with $\lambda(\tau-\tau')$ a time-dependent atomic field adjusted to make the atomic Green's function equal to the local lattice Green's function. We define an effective medium by

$$G_0^{-1}(\mathrm{i}\omega_n) = G_n^{-1} + \Sigma_n = \mathrm{i}\omega_n + \mu - \lambda_n, \tag{8}$$

with Σ_n the local self-energy and λ_n the Fourier transform of $\lambda(\tau)$. The trace in equation (4) can be evaluated directly to yield

$$G_n = w_0 G_0(\mathrm{i}\omega_n) + w_1[G_0^{-1}(\mathrm{i}\omega_n) - U]^{-1}, \tag{9}$$

with $w_0 = 1 - w_1$ and

$$w_1 = \exp[-\beta(E_f - \mu)] Z_0(\mu - U)/Z. \tag{10}$$

The self-consistency relation needed to determine λ_n and G_n is to equate the local lattice Green's function to the atomic Green's function via

$$G_n = \int_{-\infty}^{\infty} \mathrm{d}\epsilon \frac{\rho(\epsilon)}{\mathrm{i}\omega_n + \mu - \Sigma_n - \epsilon}, \tag{11}$$

with $\rho(\epsilon) = \exp(-\epsilon^2)/\sqrt{\pi}$ the noninteracting density of states for the infinite-dimensional hypercubic lattice.

The iterative algorithm to solve for G_n starts with $\Sigma_n = 0$. Then equation (11) is used to find G_n, equation (8) is employed to extract the effective medium, equation (9) is used to find a new local Green's function, and then equation (8) is used to find the new self-energy. The algorithm is then repeated until it converges, which usually requires only about a dozen or so iterations. This algorithm can also be used on the real axis (with suitably modified equations) to directly solve for the Green's function and self-energy on the real axis. Here, we examine the half-filled case $\rho_d = \sum_i \langle n_i \rangle / N = 1/2$ and $\rho_f = \sum_i \langle w_i \rangle / N = 1/2$, which corresponds to $\mu = U/2$ and $E_f = 0$.

The dynamical charge vertex is local in infinite dimensions which implies that correlation functions that have the same symmetry as the lattice are renormalized due to a nontrivial charge vertex, but correlation functions that are orthogonal to the lattice, have no vertex corrections, and so they are represented by their bare bubble diagrams [8]. In two dimensions, the Raman scattering amplitudes are typically chosen as follows:

$$\begin{aligned}
\gamma_{A_{1\mathrm{g}}}(\mathbf{k}) &\approx \frac{\partial^2 \epsilon(\mathbf{k})}{\partial k_x \partial k_x} + \frac{\partial^2 \epsilon(\mathbf{k})}{\partial k_y \partial k_y} \approx -\epsilon(\mathbf{k}), \\
\gamma_{B_{1\mathrm{g}}}(\mathbf{k}) &\approx \frac{\partial^2 \epsilon(\mathbf{k})}{\partial k_x \partial k_x} - \frac{\partial^2 \epsilon(\mathbf{k})}{\partial k_y \partial k_y} \approx \cos k_x - \cos k_y, \\
\gamma_{B_{2\mathrm{g}}}(\mathbf{k}) &\approx \frac{\partial^2 \epsilon(\mathbf{k})}{\partial k_x \partial k_y} \approx \sin k_x \sin k_y,
\end{aligned} \tag{12}$$

with $\epsilon(\mathbf{k})$ the electronic band structure. Note that the $\mathrm{B_{2g}}$ response vanishes for nearest-neighbour hopping only, which is what we consider here. The above forms can be generalized to the infinite-d limit by choosing

$$\gamma_{A_{1\mathrm{g}}}(\mathbf{k}) \approx c - \epsilon(\mathbf{k}), \quad \gamma_{B_{1\mathrm{g}}}(\mathbf{k}) \approx \frac{1}{\sqrt{d}} \sum_{i=1}^{d} (-1)^i \cos k_i, \tag{13}$$

where we include a constant term c in the $\mathrm{A_{1g}}$ amplitude, since it is allowed by symmetry.

A simple analysis in the $\mathrm{B_{1g}}$ case shows that the $\mathrm{B_{1g}}$ response does not have any vertex corrections, as expected, and that it is equal to the bare bubble. The basic argument is that we must evaluate a summation over $\mathbf{k}$ of the form

$$\sum_{\mathbf{k}} \frac{1}{\sqrt{d}} \sum_{i=1}^{d} (-1)^i \cos k_i \frac{1}{X + \frac{2}{\sqrt{d}} \sum_{j=1}^{d} \cos k_j}, \tag{14}$$

which arises when examining the Dyson equation for the B_{1g} response (and we can assume the imaginary part of X is greater than zero). Writing the fraction in equation (14) as the integral of an exponential

$$\frac{1}{X+\frac{2}{\sqrt{d}}\sum_{j=1}^{d}\cos k_j} = -\mathrm{i}\int_0^{\infty}\mathrm{d}z\exp\left[\mathrm{i}z\left(X+\frac{2}{\sqrt{d}}\sum_{j=1}^{d}\cos k_j\right)\right], \tag{15}$$

allows one to decouple the summation over momentum to the sum over d identical terms, each multiplied by $(-1)^i$. This then vanishes for all even d and for odd-d in the limit $d\to\infty$ (due to the $1/\sqrt{d}$ term). So the evaluation of the B_{1g} response reduces to the evaluation of the bare bubble. A straightforward calculation then yields

$$\chi_{B_{1g}}(\mathrm{i}\nu_l) = -\frac{T}{2}\sum_n \frac{G(\mathrm{i}\omega_n)-G(\mathrm{i}\omega_{n+l})}{\mathrm{i}\nu_l+\Sigma(\mathrm{i}\omega_n)-\Sigma(\mathrm{i}\omega_{n+l})}. \tag{16}$$

This formula can be easily analytically continued to the real axis by following the same procedure outlined in the calculation of the dynamical charge susceptibility [9]: rewrite the sum over Matsubara frequencies by a contour integral of advanced or retarded Green's functions and self-energies multiplied by the Fermi factor, and then deform the contours to the real axis picking up any poles in the complex plane. Under the assumption that there are no extra poles when the contours are deformed, one ends up with the following expression for the B_{1g} response:

$$\begin{aligned}\chi_{B_{1g}}(\nu) = \frac{-\mathrm{i}}{4\pi}\int_{-\infty}^{\infty}\mathrm{d}\omega \quad \Bigg\{ & \quad f(\omega)\frac{G(\omega)-G(\omega+\nu)}{\nu+\Sigma(\omega)-\Sigma(\omega+\nu)} \\ & - \quad f(\omega+\nu)\frac{G^*(\omega)-G^*(\omega+\nu)}{\nu+\Sigma^*(\omega)-\Sigma^*(\omega+\nu)} \\ & - \quad [f(\omega)-f(\omega+\nu)]\frac{G^*(\omega)-G(\omega+\nu)}{\nu+\Sigma^*(\omega)-\Sigma(\omega+\nu)}\Bigg\},\end{aligned} \tag{17}$$

with $f(\omega) = 1/[1+\exp(\beta\omega)]$ the Fermi function. We verify that this expression is indeed accurate, by using the spectral formula to calculate the Raman response on the imaginary axis and comparing it to the result directly calculated from the expression in equation (16). We find that the results rarely differ by more than one part in a thousand confirming the accuracy of the analytic continuation.

The A_{1g} response is more complicated, because it requires a proper treatment of the vertex contributions. Fortunately, the charge vertex for the Falicov-Kimball model is well-known [9] and assumes a simple form (for $\nu_l \neq 0$)

$$\Gamma(\mathrm{i}\omega_m,\mathrm{i}\omega_n;\mathrm{i}\nu_l) = \delta_{m,n}\frac{1}{T}\frac{\Sigma(\mathrm{i}\omega_n)-\Sigma(\mathrm{i}\omega_{n+l})}{G(\mathrm{i}\omega_n)-G(\mathrm{i}\omega_{n+l})}. \tag{18}$$

Hence, the Raman response in the A_{1g} channel can be found by solving the relevant Dyson's equation, using the above form of the charge vertex. The steps to do this are straightforward, but the algebra is somewhat cumbersome and will be presented elsewhere. The result is

$$\chi_{\mathrm{A_{1g}}}(\mathrm{i}\nu_l) = -T\sum_n \frac{\bar{\chi}_0(\mathrm{i}\omega_n;\mathrm{i}\nu_l) - [\chi_0(\mathrm{i}\omega_n;\mathrm{i}\nu_l) + G(\mathrm{i}\omega_n)G(\mathrm{i}\omega_{n+l})]T\Gamma(\mathrm{i}\omega_n,\mathrm{i}\omega_n;\mathrm{i}\nu_l)}{1+\chi_0(\mathrm{i}\omega_n;\mathrm{i}\nu_l)T\Gamma(\mathrm{i}\omega_n,\mathrm{i}\omega_n;\mathrm{i}\nu_l)}, \tag{19}$$

where the charge vertex is found in equation (18), the bare susceptibility χ_0 satisfies

$$\chi_0(\mathrm{i}\omega_n;\mathrm{i}\nu_l) = -\frac{G(\mathrm{i}\omega_n) - G(\mathrm{i}\omega_{n+l})}{\mathrm{i}\nu_l + \Sigma(\mathrm{i}\omega_n) - \Sigma(\mathrm{i}\omega_{n+l})}, \tag{20}$$

and the other bare susceptibility $\bar{\chi}_0$ (which is where all of the c dependence lies) is

$$\begin{aligned}\bar{\chi}_0(\mathrm{i}\omega_n;\mathrm{i}\nu_l) \;&=\; [-c^2(G_n - G_{n+l}) + 2c(Z_nG_n - Z_{n+l}G_{n+l}) + Z_n - Z_{n+l} \\ &\quad - Z_n^2G_n + Z_{n+l}^2G_{n+l}]/[\mathrm{i}\nu_l + \Sigma_n - \Sigma_{n+l}].\end{aligned} \tag{21}$$

Here we used the notation $Z_n = \mathrm{i}\omega_n + \mu - \Sigma(\mathrm{i}\omega_n)$.

It is a straightforward exercise to perform a similar analytic continuation of this expression, but we will not write down the result here.

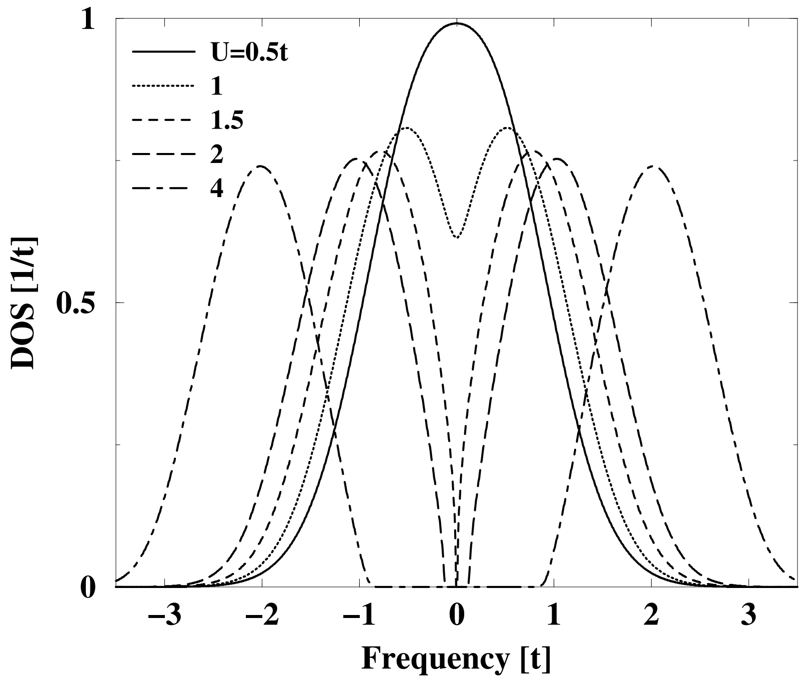

Figure 1. Interacting density of states for various values of U as indicated. The MIT occurs for $U = 1.5t$. Note the interacting DOS is independent of temperature for the Falicov-Kimball model in $d \to \infty$.

3. Results

The Falicov-Kimball model has a ground state that is not a Fermi liquid because the lifetime of a quasiparticle is finite at the Fermi energy. As U increases,

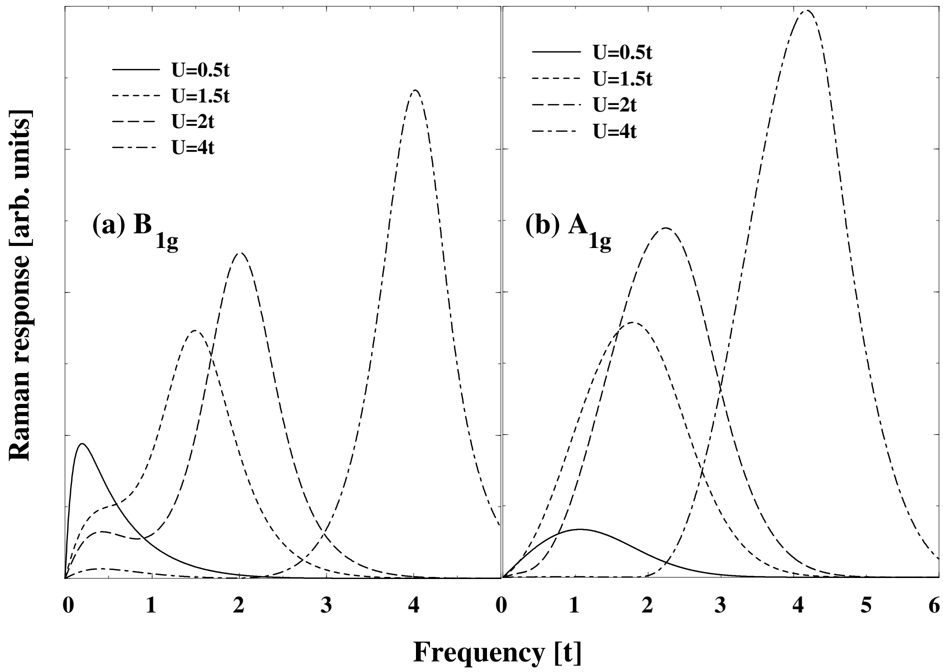

Figure 2. The Raman response (imaginary part of the Raman susceptibility) for $T = 0.5t$ for four different values of U for the (a) B_{1g} and (b) A_{1g} channels, respectively. Notice how the vertex corrections suppress the low-frequency spectral weight in the insulating phase for A_{1g} channel.

the system first enters a pseudogap phase, where spectral weight is depleted near the chemical potential, and then undergoes a metal-insulator transition [10]. The interacting density of states (DOS) is, however, temperature-independent for fixed U and fixed electron fillings.

We plot the DOS in figure 1 for values of U ranging from a weakly correlated metal $U < 0.65$, to a pseudogap phase $0.65 < U < 1.5$ to the insulator phase $U > 1.5$. The quantum critical point occurs at $U = 1.5$ where the interacting DOS is suppressed to zero at the chemical potential because a pole develops in the self-energy (the "gap region" actually has an exponentially small DOS because the hypercubic lattice has infinite tails). The corresponding imaginary part of the Raman response is plotted in figure 2 at a moderate temperature $T = 0.5t$ and various values of U. In figure 2a we show the B_{1g} response and in 2(b) we show the A_{1g} response (for $c = 0.1$). Note that the Raman scattering is quite similar for the two channels for the gross features–they both display the classic band-metal behaviour for small U, which evolves to a charge transfer peak centered at U in the large-U mode, as expected for an insulator. The B_{1g} response, however, has more low-frequency spectral weight when we are near the quantum critical point(at $U = 1.5$). The vertex corrections in the A_{1g} channel suppress these low-energy features.

In figure 3, we show the Raman response as a function of temperature for a system on the insulating side of, but close to, the quantum critical point ($U = 2$). The B_{1g} response is in figure 3a and the A_{1g} response is in figure 3b. Note how the

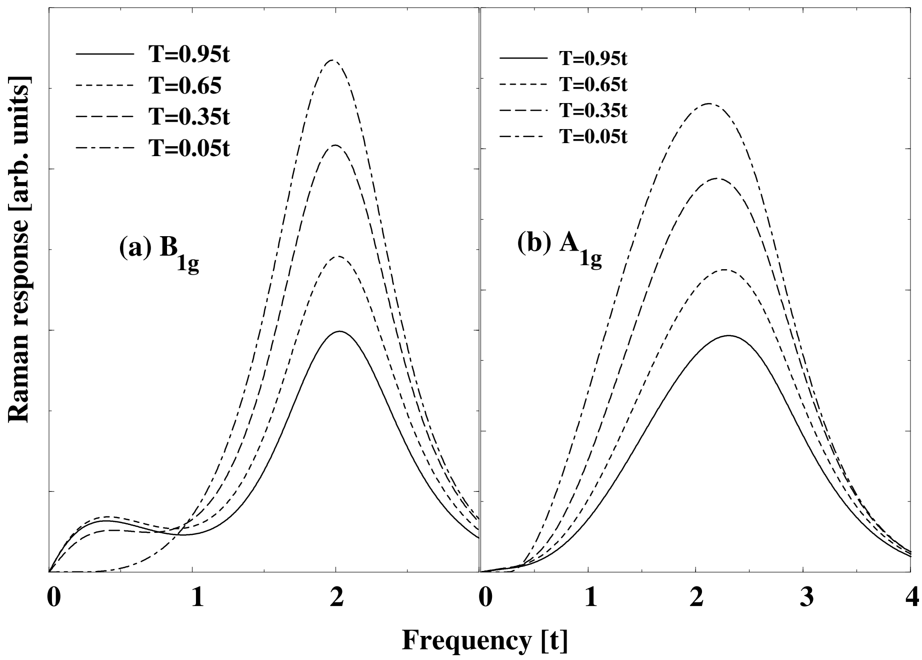

Figure 3. The Raman response (imaginary part of the Raman susceptibility) as a function of temperature for $U = 2t$ for the (a) $\mathrm{B_{1g}}$ and (b) $\mathrm{A_{1g}}$ channels, respectively. Notice how the charge-transfer peaks have similar behaviour in both channels, but that the low-frequency response is quite anomalous in the $\mathrm{B_{1g}}$ channel.

charge transfer peak feature is present at high temperatures, and steadily increases as T is lowered. The $\mathrm{B_{1g}}$ response is most interesting at low energies. The spectral feature at low energy has a strong temperature dependence that is sharply reduced as $T \to 0$. This is similar to the $\mathrm{B_{1g}}$ response seen in the cuprates. We study this phenomenon further in figures 4 and 5 which plot the normalized low-frequency spectral weight as a function of T and the inverse of the Raman slope (as $\nu \to 0$) for the $\mathrm{B_{1g}}$ channel. We arbitrarily define the low-frequency weight to be all spectral features from $\nu = 0$ to $\nu = U/2$ and the high-frequency weight to be spectral features with $\nu > U/2$. This division is obvious in the insulator phase, since the low-energy features and the high-energy features are well separated, but becomes less obvious in the pseudogap region. Note how, in all cases, the low-frequency spectral weight is sharply depleted as T is lowered, with the effect being the largest when one is well into the insulating phase. The Raman inverse slope is even more interesting. Since the Falicov-Kimball model has a temperature-independent DOS, this implies that the self-energy is also temperature-independent. Conventional reasoning would then say that the scattering rate (derived from the imaginary part of the self-energy) would be a constant, and hence, the Raman inverse slope should also be a constant, since it measures the scattering rate of the charge excitations. This is indeed true at low T for the weakly interacting systems, but is violated as we near and pass through the metal-insulator transition. This rise in the Raman inverse slope is indicative of the formation of a gap in the quasiparticle spectrum. What is interesting is that we

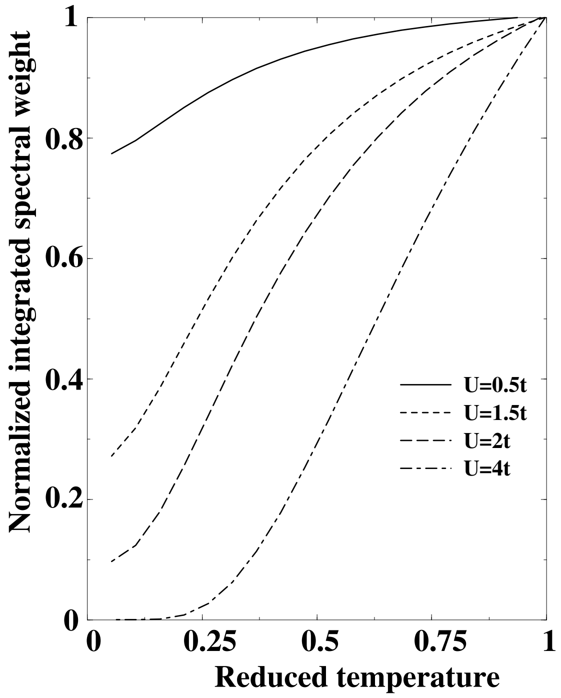

Figure 4. The integrated B_{1g} spectral weight ratio for low frequencies to high frequencies normalized to its value at $T = 0.95t$ plotted versus reduced temperature $T/0.95t$. Notice how the spectral weight is sharply depleted at low temperatures as one nears and crosses the MIT.

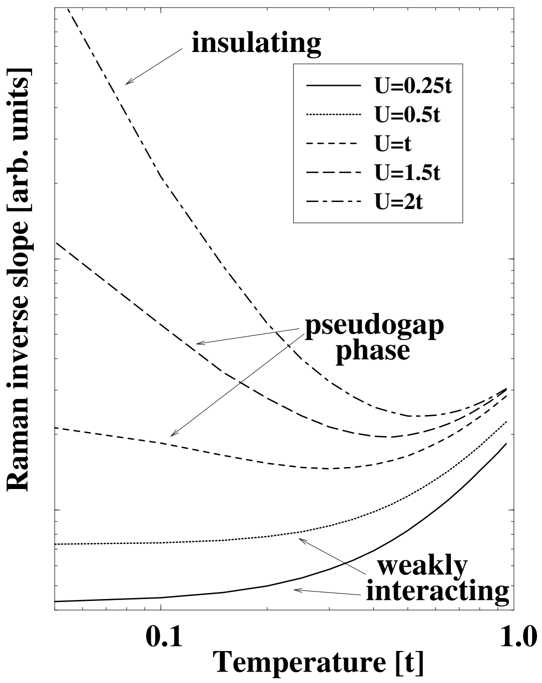

Figure 5. Log-log plot of the inverse Raman slope for the B_{1g} channel at low frequencies versus temperature for several values of U. The characteristic rise at low-T for the pseudogap and insulating phases matches well with the experimental data on the cuprates.

see a precursor effect of the insulating behaviour as we near the quantum critical point. This data compares quite well with the results seen in the underdoped cuprate materials.

4. Discussion and conclusions

There is a simple explanation to the origin of the anomalous low-frequency features of the Raman spectra in the insulating mode, but close to the quantum critical point. If we examine the integral for the B_{1g} Raman response in equation (17), we note three important points (i) the imaginary part of the Raman response is proportional to the real part of the integrand; (ii) the integrand vanishes if the Green function (and self-energy) are both real; (iii) all temperature dependence arises from the Fermi factors, since both G and Σ are temperature-independent. In the insulating mode, the DOS breaks into two pieces, a lower band centered at $-U/2$ with a width of $O(1)$ and an upper band at $U/2$ with a width of $O(1)$. The Green's functions are complex only when the frequency argument lies within one of the bands.

Hence there are two main contributions to the Raman response: (i) intraband processes, where $\omega \approx -U/2$ or $U/2$ and $\nu \approx 1$; and (ii) interband processes, where $\omega \approx -U/2$ and $\nu \approx U$. The interband processes, with $\nu \approx U$ are what give rise to the charge-transfer peaks seen in the Raman response. The intraband processes, with $\nu \approx 1$, give rise to the low-frequency spectral features. Furthermore, at low temperatures, the low-frequency features are proportional to $f(\omega) - f(\omega+\nu)$ which can be approximated by $\exp(-U/2T)[1-\exp(\nu/T)]$. Hence, we expect a Raman inverse slope to act like $T\exp(U/2T)$ and the low-frequency spectral weight should go like $\exp(-U/2T)$, which can explain the features seen in our results. In the A_{1g} channel, the charge vertex makes the integrand more complicated to evaluate, and the vertex corrections end up suppressing the low-frequency response.

Since the form for the B_{1g} response is identical in other single-band models, like the Hubbard model, we expect that the B_{1g} Raman response will be essentially the same as seen for the Falicov-Kimball model. The only modifications are that the DOS now has T-dependence, which will relax criterion (iii) above, and that the system has a Fermi-liquid ground state for low temperatures and small to moderate U. Nevertheless, in the insulating mode, the DOS will separate into an upper and lower Hubbard band, and the analysis given above will hold for determining the low-T features, so we expect to see the same anomalous low-frequency behaviour in the B_{1g} channel as is seen here. We cannot make a similar comment about the A_{1g} channel, because the charge vertex will no longer assume the simple form for the Falicov-Kimball model, and the vertex corrections can modify the results, but we don't expect there to be much qualitative difference there either.

The calculations presented here are remarkably similar to those observed in the B_{1g} channel in the normal state of the cuprates [1]. As the doping in these materials is reduced from the overdoped side to the underdoped side of the phase diagram, the B_{1g} Raman spectra deviate strongly from our expectations for metallic behaviour. A large depletion of spectral weight at low frequencies is observed for B_{1g} with underdoping, with a concommitant shift of spectral weight out to two-magnon energies ~ 2700 cm^{-1}. For a given temperature, the integrated low-frequency spectral weight in the B_{1g} channel falls by over an order of magnitude from overdoped to underdoped. Both of these features are similar to our observations shown in figures 2–4. This is indicative of the formation of a pseudogap which affects the B_{1g} quasiparticles and sets in well before the metal-insulator transition is reached. The inverse Raman slope is found to increase with doping at a given temperature and, moreover, has a strong upturn with decreasing temperature in the more underdoped systems, qualitatively similar to our figure 5. Again, since we believe our model captures the salient features of Raman scattering in the vicinity of a quantum critical point, the Raman data from the cuprates directly shows the influence on the B_{1g} quasiparticles by the underlying metal-insulator transition.

In summary, we have examined the Raman response of a system that goes through a metal-insulator transition exactly, using the dynamical mean field theory for the spinless Falicov-Kimball model. Our results provide a continuous interpolation between the known metallic and insulating Raman responses. The results of this model system should be qualitatively similar to those of other correlated models that require quantum Monte Carlo simulation to solve (such as the Hubbard and Holstein models), and display the qualitative features seen in the cuprates.

5. Acknowledgments

We acknowledge useful discussions with Lance Cooper, Rudi Hackl, J.C.Irwin, Miles Klein, Paul Miller, and Andrij Shvaika. J.K.F. acknowledges support from the National Science Foundation under grant number DMR–9973225. He also acknowledges the hospitality of the Newton Institute where some of this work was completed in June of 2000. T.P.D. acknowledges support from the National Science and Engineering Research Council of Canada. This work was supported in part by Award No. UW0–1012 of the U.S. Civilian Research and Development Foundation for the Independent States of the former Soviet Union (CRDF).

References

1. Chen X.K., Naeini J.G., Hewitt K.C., Irwin J.C., Liang R., Hardy W.N. Electronic Raman scattering in underdoped $YBa_2Cu_3O_{6.5}$. // Phys. Rev. B, 1997, vol. 56, p. R513; Naeini J.G., Chen X.K., Irwin J.C., Okuya M., Kimura T., Kishio K. Doping dependence of the pseudogap in $La_{2-x}Sr_xCuO_4$. // Phys. Rev. B, 1999, vol. 59, p. 9642; Rübhausen M., Hammerstein O.A., Bock A., Merkt U., Rieck C.T., Guptasarma P., Hinks D.G., Klein M.V. Doping dependence of the electronic interactions in Bi-2212 cuprate superconductors: doped antiferromagnets or antiferromagnetic fermi liquids? // Phys. Rev. Lett., 1999, vol. 82, p. 5349; Opel M., Nemetschek R., Hoffmann C., Philipp R., Müller P.F., Hackl R., Tütto I., Erb A., Revaz B., Walker E., Berger H., Forró L. Carrier relaxation, pseudogap, and superconducting gap in high-T_c cuprates: A Raman scattering study. // Phys. Rev. B, 2000, vol. 61, p. 9752.
2. Platzmann P.M., Tzoar N. Nonlinear interaction of light in a plasma. // Phys. Rev., 1964, vol. 136, p. A11.
3. Chubukov A.V., Frenkel D.M. Resonant two-magnon Raman scattering in parent compounds of high T_c superconductors. // Phys. Rev. B, 1995, vol. 52, p. 9760.
4. Falicov L.M., Kimball J.C. Simple model for semiconductor-metal transitions: SmB_6 and transition-metal oxides. // Phys. Rev. Lett., 1969, vol. 22, p. 997.
5. Metzner W., Vollhardt D. Correlated lattice fermions in $d = \infty$ dimensions. // Phys. Rev. Lett., 1989, vol. 62, p. 324.
6. Brandt U., Mielsch C. Thermodynamics and correlation functions of the Falicov-Kimball model in large dimensions. // Z. Phys. B, 1989, vol. 75, p. 365; Thermodynamics of the Falicov-Kimball model in large dimensions. II. Critical temperature and order parameter. // Z. Phys. B, 1990, vol. 79, p. 295.
7. Freericks J.K. Spinless Falicov-Kimball model (annealed binary alloy) from large to small dimensions. // Phys. Rev. B, 1993, vol. 47, p. 9263; Freericks J.K., Zlatić V. Anomalous magnetic response of the spin-one-half Falicov-Kimball model. // Phys. Rev. B, 1998, vol. 58, p. 322.
8. Khurana A. Electrical conductivity in the infinite-dimensional Hubbard model. // Phys. Rev. Lett., 1990, vol. 64, p. 1990.

9. Shvaika A.M. Dynamical susceptibilities in strong coupling approach. // Physica C, 2000, vol. 341–348, p. 177; Freericks J.K., Miller P. Dynamical charge susceptibility of the spinless Falicov-Kimball model. // Phys. Rev. B, 2000, vol. 62, p 10022.
10. Van Dongen P.G.J., Leinung C. Mott-Hubbard transition in a magnetic field. // Ann. Phys. (Leipzig), 1997, vol. 6, p. 45.
11. Van Dongen P.G.J. Exact mean-field theory of the extended simplified Hubbard model. // Phys. Rev. B, 1992, vol. 45, p. 2267.

Нерезонансне комбінаційне розсіяння при проходженні переходу метал-ізолятор: точний аналіз моделі Фалікова-Кімбала

Дж.К.Фрірікс [1,2], Т.П.Деверо [3]

[1] Фізичний факультет, Університет Джорджтауну, Вашінгтон, округ Колумбія 20057, США

[2] Інститут Ісаака Ньютона, Кембрідж CB3 0EH, Великобританія

[3] Фізичний факультет, Університет Ватерлоо, Ватерлоо, Онтаріо, Канада, N2l 3G1

Отримано 14 серпня 2000 р.

Упродовж років теорія комбінаційного розсіяння (КР) обмежувалася розглядом або ізоляторів або суто металічного стану. Хоча можна багато довідатися, зосередивши увагу тільки на металах чи ізоляторах, останні експериментальні роботи з купратних систем вказують на бажаність формулювання теорії раманівського відгуку, яке придатне при проходженні через квантову критичну точку - перехід метал-ізолятор (ПМІ). Використовуючи модель Фалікова-Кімбала як канонічну модель ПМІ, ми застосовуємо теорію динамічного середнього поля для побудови точної теорії нерезонансного КР. Зокрема, ми розглядаємо утворення піків, зумовлених переносом заряду, та псевдощілин, а також низькоенергетичну динаміку. Результати якісно зіставимі з експериментальними B_{1g} спектрами КР у купратах, в яких фіксують "гарячі" квазічастинки вздовж осей зони Брілюена. Результати дають важливу інформацію про електронний транспорт у нормальному стані та псевдощілину в купратах.

Ключові слова: *комбінаційне розсіяння, перехід метал-ізолятор*

PACS: *78.30.-j, 71.30.+h, 74.72.-h*